Journal of Scientific Computing (2020) 82:51
https://doi.org/10.1007/s10915-020-01155-7

Numerical Resolution of a Three Temperature Plasma Model

C. Enaux[1] · S. Guisset[1] · C. Lasuen[1] · Q. Ragueneau[1]

Received: 28 May 2019 / Revised: 20 November 2019 / Accepted: 2 February 2020

Abstract
This paper is devoted to the numerical approximation of a three temperature plasma model: one for the ions, one for the electrons and one for the radiation (photons). A reformulation of the model is proposed that allows to build a convex combination-based scheme that unconditionally satisfies a maximum principle, at each sub-iteration of the non-linear iterative process. This yields a very robust scheme that can handle stiff source terms. In addition, the methodology is extended to include the contribution of a radiative flux (Rosseland diffusion approximation) and electronic and ionic conductivities (Spitzer–Härm diffusion approximation). Several numerical results are carried out to demonstrate the interest of the numerical approach.

Keywords Three temperature model · Numerical schemes · Plasma physics · Radiative transfer · Non-equilibrium radiation diffusion

Mathematics Subject Classification 65M12 · 35Q35 · 82D10 · 82A25

1 Introduction

Background
The relaxation between the electronic and ionic temperatures toward the same temperature happens on time scales larger than the ones involved to reach quasi-neutral regimes or required for the electron and ion distribution functions to reach Maxwellian equilibrium distributions [1]. This point has some importance since in many practical applications, such as astrophysics [10] or inertial confinement fusion [7], the characteristic times of interest can be of the same order of the temperature relaxation times. When this is the case, a two-temperature hydrodynamics model is required [1]. In addition, in the presence of strong radiative effects, the modeling of photon transport is also required. To address this issue, different models are available depending on the required level of accuracy [11]. In the present work, we restrict

✉ S. Guisset
sebastien.guisset@cea.fr

C. Enaux
cedric.enaux@cea.fr

[1] CEA, DAM, DIF, 91297 Arpajon, France

Published online: 12 February 2020

ourselves to the study of a gray-diffusion model. However, the presented methodology can be extended to multi-group and/or transport models. This will be investigated in the future.

The discretisation of such radiation-hydrodynamic models has been largely investigated. When the applications require a transport-type modeling, one of the most used methods to simulate thermal radiation propagation is the Implicit Monte-Carlo method. Early studies can be found in [6] where the Implicit Monte-Carlo method is applied to a two-temperature model (only one equilibrium temperature is considered for matter). We also refer to [3] where the Implicit Monte-Carlo method is extended to the study of three temperature models and several numerical approaches are presented and compared for describing the coupling between radiation, electron and ion energies. We also mention the work [16] in which an estimator of the time step is proposed in order to satisfy a discrete maximum principle since Implicit Monte-Carlo methods can produce nonphysical overshoots of material temperatures when large time steps are used [9].

If the applications under consideration allow diffusion-type approximations, standard Newton-Raphson or fix point algorithms are also widely used to solve three temperature models [13]. While iterative numerical strategies to deal with non-linear source terms are forbidden when working with Implicit Monte-Carlo method, they can be very effective here. We refer to [4] for numerical comparisons between several simulation codes for solving three temperature models. Here, we also mention [5,12] and the references therein where Jacobian-free Newton-Krylov methods are considered to derive efficient algorithms for radiation diffusion equations. It should be noticed that the time integration of non-equilibrium radiation diffusion models has been largely investigated in [8] and references therein. Because of the stiffness of the different physical terms, a careful numerical analysis is required before considering linearisation or operator splitting strategies. We stress the numerical difficulties encountered when dealing with stiff and nonlinear source terms with enough accuracy and stable discretisations.

Present approach and outline

The present work introduces a numerical approach that differs from all the previous studies: a model reformulation is proposed that allows to build a convex combination-based scheme that unconditionally satisfies a maximum principle at each sub-iteration of the non-linear iterative process. This yields a very robust three temperature scheme that can handle stiff source terms. In addition, the methodology is extended to include the contribution of a radiative flux (Rosseland diffusion approximation) and electronic and ionic conductivities (Spitzer–Härm diffusion approximation). The originality of this work does not come from the temporal discretisation which relies on standard implicit–explicit strategies. However, we believe the original idea comes from the reformulation of the model with matched T^4 function (Sect. 2.3). Indeed, this linearisation allows the derivation of schemes with strong L^∞ stability properties among other fundamental properties such as energy conservation, asymptotic-preserving. In addition, it is shown that the different coefficients involved in the reformulation are never singular (coefficients β_α and δ_{ie}) and carefully set to enforce a correct energy conservation. A convergence result (under CFL condition) of the method proposed is also provided. We point out that a direct discretisation of the initial model using a standard Newton-Raphson algorithm does not ensure a discrete maximum principle at each sub-iteration. Even if at convergence the correct solutions can be obtained, during the iterative process the temperature profiles are not bounded and may for example become negative. In a second part, the 1D extension is studied and the different scheme properties are clearly stated. We believe the methodology presented here naturally extend to multi-dimension settings.

The paper is organized as follows. We start by introducing the studied set of governing equations with its main properties. In order to prepare the derivation of an efficient numerical scheme, a reformulation of the model is presented. Next, in the 0D case (no spatial variation), the scheme is derived and strong properties are proved. Finally, the procedure is extended to the 1D slab case to include the radiative flux. Several iterative methods are proposed and compared. The contributions of the electronic and ionic conductivities are also included. Several numerical tests are carried out to illustrate the efficiency of the numerical approach.

2 Governing Equations and Reformulation

2.1 Set of Equations

In the present work a hot plasma made of ions, electrons and photons is considered. The hydrodynamic evolution of the particles is chosen at rest (mass and momentum evolution) and we focus on the energy evolution of each particle population. This approximation is relevant in applications where the material motion can be neglected or, can be removed by appropriate operator splitting strategies. In this framework, we consider that the energy evolution of photons (radiation), electrons and ions can be respectively described by the following set of equations

$$\begin{cases} \partial_t E_r + \nabla \cdot \mathbf{F}_r = c\sigma_P(aT_e{}^4 - E_r) + Q_r, \\ \partial_t E_e + \nabla \cdot \mathbf{F}_e = c\sigma_P(E_r - aT_e{}^4) + c\kappa(T_i - T_e) + Q_e, \\ \partial_t E_i + \nabla \cdot \mathbf{F}_i = c\kappa(T_e - T_i) + Q_i, \end{cases} \tag{1}$$

where E_r, E_e and E_i are respectively the radiative, electronic and ionic energy densities. The electronic, ionic temperatures are respectively written T_e and T_i and the radiative temperature T_r is defined by $E_r = aT_r^4$. The speed of light c and Stefan constant a are strictly positive. The absorption opacity σ_P (P for Planck) is assumed to be a given non-linear function of T_e and T_r. κ is a positive relaxation coefficient of the electronic and ionic temperatures which non-linearly depends on T_e and T_i. Finally $\mathbf{F}_r$, $\mathbf{F}_i$ and $\mathbf{F}_r$ are energy fluxes. Although the set of equations (1) is general, we restrict ourselves to the diffusion approximation framework whereby

- Rosseland diffusion approximation is considered for the photons. Where the radiative flux is [11]
$$\mathbf{F}_r = -\frac{c}{3\sigma_R}\nabla E_r, \tag{2}$$
where the Rosseland opacity σ_R depends non linearly on T_e and T_r.
- Spitzer–Härm diffusion approximation is used for the electronic and ionic thermal conductivities. Assuming ions and electrons distributions are local Maxwellians [14], the electronic and ionic thermal conductivities are written as
$$\mathbf{F}_\alpha = -\lambda_\alpha^{'}\nabla T_\alpha, \qquad \lambda_\alpha^{'} = K_\alpha T_\alpha^{5/2}, \qquad \alpha = e, i, \tag{3}$$
where K_e and K_i are plasma depending coefficients. We now define the heat capacities $C_{v,\alpha}$ as
$$\frac{dE_\alpha}{dT_\alpha} = \rho C_{v,\alpha}(T_\alpha) \qquad \text{with} \qquad \alpha = e, i, \tag{4}$$
where ρ is the mass density of the fluid which is here restricted to be constant in time but non-uniform in space.

2.2 Model Properties

The main model properties of interest here are

- Total energy conservation.

Adding the three equations of (1) leads to the following total energy balance law

$$\partial_t(E_i + E_e + E_r) + \nabla \cdot (\mathbf{F}_i + \mathbf{F}_e + \mathbf{F}_r) = Q_i + Q_e + Q_r. \tag{5}$$

In the absence of source terms (i.e. $Q_\alpha = 0,\ \forall \alpha$), Eq. (5) is a conservation law.

- Maximum principle.

In the case with no source term ($Q_\alpha = 0,\ \forall \alpha$), if the electronic, ionic and radiative temperatures are bounded at the initial time and at the boundaries then they remain bounded at all time. More precisely if

$$\max(T_e(t=0,x), T_i(t=0,x), T_r(t=0,x)) \leq K,$$

for $K \in \mathbb{R}^+_\star$ then

$$\max(T_e(t,x), T_i(t,x), T_r(t,x)) \leq K \qquad \forall t \in \mathbb{R}^+.$$

Such a property is studied in [9] and references therein.

- Stability of the state $T_i = T_e = T_r$.

In the 0D case (no spatial variation) with no source term, all states such that $T_i = T_e = T_r$ are equilibrium states (see "Appendix").

- Asymptotic behavior in the limit where σ_P and κ tend to infinity.

Let τ be the characteristic time of evolution and ε the dimensionless quantity

$$\varepsilon = 1/\max(c\sigma_P\tau, \kappa\tau),$$

to be eventually made vanishingly small. Scaling the set of Eq. (1) with τ and letting ε tend to zero gives to first order in ε (by using a standard Hilbert expansion)

$$T_i^0 = T_e^0 = T_r^0 = T_{eq},$$

where index zero indicates the first order term in the Hilbert decomposition. In addition, the time evolution of T_{eq} (obtained by adding the three energy equation at next order in ε) is given by

$$\partial_t(E_i(T_{eq}) + E_e(T_{eq}) + E_r(T_{eq})) + \nabla \cdot (\mathbf{F}_i(T_{eq}) + \mathbf{F}_e(T_{eq}) + \mathbf{F}_r(T_{eq})) = Q_i + Q_e + Q_r.$$

This last equation is called the (one temperature) equilibrium diffusion limit.

2.3 Model Recasting with Matched T^4 Functions

In order to prepare the derivation of a suitable numerical scheme, a reformulation of the model (1) is here suggested. For clarity, this model recasting is presented here in the 0D case (no spatial variation). The complete model will be studied in the next sections. We highlight that this procedure is not trivial and is one of the key points for the derivation of an adapted

numerical scheme. Here, model (1) is expressed for the variables $\phi_\alpha = aT_\alpha^4$, where $\alpha = r$, e, i. Note that $E_r = \phi_r = aT_r^4$. Using these notations one first has

$$\begin{cases} \partial_t \phi_r = c\sigma_P(\phi_e - \phi_r) + Q_r, \\ \partial_t E_e = c\sigma_P(\phi_r - \phi_e) + c\kappa(T_i - T_e) + Q_e, \\ \partial_t E_i = c\kappa(T_e - T_i) + Q_i. \end{cases} \tag{6}$$

The temporal derivatives of the electronic and ionic energy can be expressed as function of the temporal derivatives of ϕ_e and ϕ_i since

$$\partial_t E_\alpha = \frac{dE_\alpha}{d\phi_\alpha}\partial_t \phi_\alpha = \frac{1}{\beta_\alpha}\partial_t \phi_\alpha, \qquad \alpha = e, i$$

where

$$\beta_\alpha = \frac{d\phi_\alpha}{dE_\alpha} = \frac{d\phi_\alpha}{dT_\alpha}\frac{dT_\alpha}{dE_\alpha} = \frac{4aT_\alpha^3}{\rho C_{v,\alpha}} > 0. \tag{7}$$

Moreover, the $(T_i - T_e)$ relaxation term may be expressed differently[1] by introducing δ_{ie}

$$\delta_{ie} = \frac{T_i - T_e}{\phi_i - \phi_e},$$

that satisfies the two properties

Property 1 *The parameter δ_{ie} is always positive.*

Proof By using the definition of $\phi_\alpha = aT_\alpha^4$ (with $\alpha = e, i, r$) (which is an increasing function of T_α) gives the result. Indeed if $T_i \geq T_e$ then $\phi_i \geq \phi_e$ and if $T_i \leq T_e$ then $\phi_i \leq \phi_e$. □

Property 2 *In the limit $\phi_i - \phi_e$ tends to zero, the parameter δ_{ie} is not singular.*

Proof A direct Taylor expansion in the small parameter $\phi_i - \phi_e$ and using the definition of the parameter δ_{ie} directly gives

$$\lim_{\substack{T_i \to T, \\ T_e \to T,}} \delta_{ie} = \frac{1}{4aT^3} > 0.$$

□

Finally, the model is recast in the quasi-linear form

$$\begin{cases} \partial_t \phi_r = c\sigma_P(\phi_e - \phi_r) + Q_r, \\ \partial_t \phi_e = \beta_e c\sigma_P(\phi_r - \phi_e) + \beta_e c\kappa\delta_{ie}(\phi_i - \phi_e) + \beta_e Q_e, \\ \partial_t \phi_i = \beta_i c\kappa\delta_{ie}(\phi_e - \phi_i) + \beta_i Q_i. \end{cases} \tag{8}$$

As shown in the next section, the model is now amenable to an efficient discretization. Of course, the model (8) remains nonlinear because of the functions σ_P, κ, σ_R, β_α and δ. In addition, because of the stiffness of the different terms, fully implicit time treatments are mandatory in order to keep reasonable time steps. Indeed, in the regimes under study different stiffness in the set of equations appear, requiring a careful stability analysis.

[1] This simple trick, that will allow to build an unconditionally stable scheme, is new to our knowledge.

3 Numerical Analysis in the 0D Case (No Spatial Variation)

We start the numerical section considering the 0D case (no spatial variation) without source terms. In this setting, system (8) simplifies into

$$\begin{cases} \partial_t \phi_r = c\sigma_P(\phi_e - \phi_r), \\ \partial_t \phi_e = \beta_e c\sigma_P(\phi_r - \phi_e) + \beta_e c\kappa\delta_{ie}(\phi_i - \phi_e), \\ \partial_t \phi_i = \beta_i c\kappa\delta_{ie}(\phi_e - \phi_i). \end{cases} \tag{9}$$

3.1 Numerical Scheme

The temporal discretisation chosen consist in a standard backward-Euler scheme. The time step is written $\Delta t = t^{n+1} - t^n$ and the quantities considered at time t^n are denoted by the index n. For more clarity, the quantities σ_P and κ are written as constant quantities in (10). However, in practice they are nonlinear function of the temperatures. Their time discretisation is discussed in "Appendix 1". The time discretisation of (9) reads

$$\begin{cases} \phi_r^{n+1} = \phi_r^n + \Delta t c\sigma_P(\phi_e^{n+1} - \phi_r^{n+1}), \\ \phi_e^{n+1} = \phi_e^n + \Delta t \beta_e^{n+1} c\sigma_P(\phi_r^{n+1} - \phi_e^{n+1}) + \beta_e^{n+1} c\kappa\delta_{ie}^{n+1}(\phi_i^{n+1} - \phi_e^{n+1}), \\ \phi_i^{n+1} = \phi_i^n + \beta_i^{n+1} c\kappa\delta_{ie}^{n+1}(\phi_e^{n+1} - \phi_i^{n+1}). \end{cases} \tag{10}$$

with

$$\delta_{ie}^{n+1} = \frac{T_i^{n+1} - T_e^{n+1}}{\phi_i^{n+1} - \phi_e^{n+1}},$$

and where the discretisation of β_α is

$$\beta_\alpha^{n+1} = \frac{\phi_\alpha^{n+1} - \phi_\alpha^n}{E_\alpha^{n+1} - E_\alpha^n}. \tag{11}$$

This choice of discretisation for the coefficient β_α^{n+1} is justified by the following arguments. We start, setting

$$\mathcal{I}_\alpha = \int_{t^n}^{t^{n+1}} \partial_t E_\alpha dt = E_\alpha(t^{n+1}) - E_\alpha(t^n).$$

Here, we point out that in order to make the model quasi-linear we work with the variables ϕ_α so that we have the requirement that $\mathcal{I}_\alpha/\Delta t$ is approached by

$$\frac{\mathcal{I}_\alpha}{\Delta t} \approx \frac{1}{\beta_\alpha^{n+1}} \frac{\phi_\alpha^{n+1} - \phi_\alpha^n}{\Delta t}. \tag{12}$$

Now, one can think in "the best" discretisation of β_α^{n+1}. A possible condition is to ensure that the numerical approximation (12) is exact. Consequently, it follows that

$$\beta_\alpha^{n+1} = \frac{\phi_\alpha^{n+1} - \phi_\alpha^n}{E_\alpha(t^{n+1}) - E_\alpha(t^n)}.$$

Finally the definition (11) is considered.

Remark It will be shown in Sect. (3.3) that the discretisation considered for the coefficient β_α enables to prove an important energy conservation property.

Now, in order to numerically solve the one-step fully implicit scheme (10), we propose the following iterative linear-implicit method

$$\begin{cases} \phi_r^{n+1,k+1} = \phi_r^n + \Delta t c\sigma_P(\phi_e^{n+1,k+1} - \phi_r^{n+1,k+1}), \\ \phi_e^{n+1,k+1} = \phi_e^n + \Delta t \beta_e^{n+1,k} c\sigma_P(\phi_r^{n+1,k+1} - \phi_e^{n+1,k+1}) \\ +\delta_{ie}^{n+1,k}\beta_e^{n+1,k} c\kappa(\phi_i^{n+1,k+1} - \phi_e^{n+1,k+1}), \\ \phi_i^{n+1,k+1} = \phi_i^n + \Delta t \delta_{ie}^{n+1,k}\beta_i^{n+1,k} c\kappa(\phi_e^{n+1,k+1} - \phi_i^{n+1,k+1}), \end{cases} \tag{13}$$

where $\phi_\alpha^{n+1,k}$ denotes the k^{th} sub-iteration at time t^{n+1} for quantity ϕ_α and we define

$$\delta_{ie}^{n+1,k} = \frac{T_i^{n+1,k} - T_e^{n+1,k}}{\phi_i^{n+1,k} - \phi_e^{n+1,k}}, \qquad \beta_\alpha^{n+1,k} = \frac{\phi_\alpha^{n+1,k} - \phi_\alpha^n}{E_\alpha^{n+1,k} - E_\alpha^n} \qquad \text{for} \qquad \alpha = e, i. \tag{14}$$

This numerical procedure is used at each time step t^n until convergence of ϕ_r, ϕ_e and ϕ_i is reached.

3.2 Practical Numerical Resolution

In order to make the numerical resolution more explicit and to prepare the numerical analysis, the scheme is rewritten under the form of convex combinations. Here, for clarity we drop index $n+1$ in the notations (but we keep it for ϕ_α).

We start by rewriting the third equation of (13) as the convex combination

$$\phi_i^{n+1,k+1} = h^k \phi_i^n + (1 - h^k)\phi_e^{n+1,k+1}, \tag{15}$$

where

$$h^k = \frac{1}{1 + \delta_{ie}^k \beta_i^k c\kappa \Delta t} \qquad \in [0, 1]. \tag{16}$$

Now, inserting Eq. (15) into the second equation of (13) one deduces

$$\phi_e^{n+1,k+1} = f^k(g^k \phi_e^n + (1 - g^k)\phi_i^n) + (1 - f^k)\phi_r^{n+1,k+1}, \tag{17}$$

where

$$f^k = \frac{1}{1 + g^k \beta_e^k c\sigma_P \Delta t} \qquad \in [0, 1], \qquad g^k = \frac{1}{1 + h^k \delta_{ie}^k \beta_e^k c\kappa \Delta t} \qquad \in [0, 1]. \tag{18}$$

Finally, Eq. (17) is inserted into the first equation of (13) to obtain the following expressions

$$\phi_r^{n+1,k+1} = j^k \phi_r^n + (1 - j^k)(g^k \phi_e^n + (1 - g^k)\phi_i^n),$$

with

$$j^k = \frac{1}{1 + f^k c\sigma_P \Delta t} \qquad \in [0, 1]. \tag{19}$$

Finally, the scheme writes under the following compact form

$$\begin{cases} \phi_r^{n+1,k+1} = j^k \phi_r^n + (1 - j^k)(g^k \phi_e^n + (1 - g^k)\phi_i^n), \\ \phi_e^{n+1,k+1} = f^k(g^k \phi_e^n + (1 - g^k)\phi_i^n) + (1 - f^k)\phi_r^{n+1,k+1}, \\ \phi_i^{n+1,k+1} = h^k \phi_i^n + (1 - h^k)\phi_e^{n+1,k+1}, \end{cases} \tag{20}$$

where f^k, g^k, h^k and j^k are defined by (16), (18) and (19). This form can be completely explicited to make appear convex combinations as the following

$$\phi_r^{n+1,k+1} = j^k \phi_r^n + g^k(1 - j^k)\phi_e^n + (1 - g^k)(1 - j^k)\phi_i^n,$$

$$\begin{aligned}
\phi_e^{n+1,k+1} &= j^k(1-f^k)\phi_r^n + (f^k g^k + (1-f^k)(1-j^k)g^k)\phi_e^n \\
&\quad + (f^k(1-g^k) + (1-f^k)(1-j^k)(1-g^k))\phi_i^n, \\
\phi_i^{n+1,k+1} &= ((1-h^k)(1-f^k)j^k)\phi_r^n \\
&\quad + ((1-h^k)(f^k g^k + (1-f^k)(1-j^k)g^k))\phi_e^n \\
&\quad + (h^k + (1-h^k)(f^k(1-g^k) + (1-f^k)(1-j^k)(1-g^k)))\phi_i^n.
\end{aligned}$$

One can check that the quantities $\phi_\alpha^{n+1,k+1}$ write as convex combinations of ϕ_α^n. In the next section, it is demonstrated that this key point enables the proof of strong stability properties.

3.3 Scheme Properties

In this section the different properties of the scheme are proved.

Property 3 *At convergence, the numerical scheme* (20) *conserves the discrete total energy.*

Proof Adding the three equations of (13) gives

$$\frac{\phi_r^{n+1,k+1} - \phi_r^n}{\Delta t} + \frac{1}{\beta_e^k}\frac{\phi_e^{n+1,k+1} - \phi_e^n}{\Delta t} + \frac{1}{\beta_i^k}\frac{\phi_i^{n+1,k+1} - \phi_i^n}{\Delta t} = 0.$$

Now, considering the expression of β_e^k and β_i^k given in (14) gives

$$\frac{\phi_r^{n+1,k+1} - \phi_r^n}{\Delta t} + \frac{E_e^{n+1,k} - E_e^n}{\phi_e^{n+1,k} - \phi_e^n}\frac{\phi_e^{n+1,k+1} - \phi_e^n}{\Delta t} + \frac{E_i^{n+1,k} - E_i^n}{\phi_i^{n+1,k} - \phi_i^n}\frac{\phi_i^{n+1,k+1} - \phi_i^n}{\Delta t} = 0 \quad (21)$$

At convergence ($k \to \infty$, $\phi_\alpha^{n+1,k+1} \to \phi_\alpha^{n+1}$ and $E_\alpha^{n+1,k+1} \to E_\alpha^{n+1}$) (a convergence result under CFL condition is given in Property 7) Eq. (21) simplifies into

$$E_r^{n+1} - E_r^n + E_e^{n+1} - E_e^n + E_i^{n+1} - E_i^n = 0,$$

leading to the energy conservation property

$$E_r^{n+1} + E_e^{n+1} + E_i^{n+1} = E_r^n + E_e^n + E_i^n.$$

□

Remark Note that the choice of the discretisation of β_α given in (14) is mandatory to obtain this discrete energy conservation property.

Property 4 (Strong stability property)
Each sub-iteration k is unconditionally L^∞ stable.

Proof The demonstration of this stability property lies in the writing of the scheme under the form of convex combinations (20). We also point out that this is only possible thanks to the reformulation of the model presented in the previous section. Now, supposing that the quantities ϕ_α^n are bounded, we introduce

$$\phi_{min}^n = \min(\phi_r^n, \phi_e^n, \phi_i^n), \quad \phi_{max}^n = \max(\phi_r^n, \phi_e^n, \phi_i^n).$$

Therefore, the first equation of (20) gives

$$j^k\phi_{min}^n + (1-j^k)g^k\phi_{min}^n + (1-j^k)(1-g^k)\phi_{min}^n \le \phi_r^{n+1,k+1}$$

$$\leq j^k \phi_{max}^n + (1-j^k) g^k \phi_{max}^n + (1-j^k)(1-g^k)\phi_{max}^n,$$

which simplifies into

$$\phi_{min}^n \leq \phi_r^{n+1,k+1} \leq \phi_{max}^n.$$

The same procedure applies for the second and third equations of (20) giving the same result for $\phi_e^{n+1,k+1}$ and $\phi_i^{n+1,k+1}$. □

Remark Taking into account of external source terms the numerical scheme proposed reads as follow

$$\begin{cases} \phi_r^{n+1,k+1} = j^k \psi_r^{n,k} + (1-j^k)(g^k \psi_e^{n,k} + (1-g^k)\psi_i^{n,k}), \\ \phi_e^{n+1,k+1} = f^k (g^k \psi_e^{n,k} + (1-g^k)\psi_i^{n,k}) + (1-f^k)\phi_r^{n+1,k+1}, \\ \phi_i^{n+1,k+1} = h^k \psi_i^{n,k} + (1-h^k)\phi_e^{n+1,k+1}. \end{cases} \tag{22}$$

where

$$\psi_r^{n,k} = \psi_r^n = \phi_r^n + Q_r \Delta t, \quad \psi_e^{n,k} = \phi_e^n + \beta_e^k Q_e \Delta t, \quad \psi_i^{n,k} = \phi_i^n + \beta_i^k Q_i \Delta t.$$

The quantities $\phi_\alpha^{n+1,k+1}$ still write as convex combinations of $\psi_\alpha^{n,k}$ so that the stability property is still verified.

Property 5 *The numerical scheme* (20) *is asymptotic-preserving in the limit* σ_P *and* κ *tend to infinity.*

Proof Let τ be the characteristic time of evolution and ε the dimensionless quantity

$$\varepsilon = 1/\max(c\sigma_P \tau, c\kappa\tau),$$

to be eventually made vanishingly small. Scaling the set of Eq. (13) with τ and letting ε tend to zero gives at first order in ε (by using a standard Hilbert expansion)

$$\phi_i^{k+1,0} = \phi_e^{k+1,0} = \phi_r^{k+1,0},$$

which by definition of ϕ_α is equivalent to

$$T_i^{k+1,0} = T_e^{k+1,0} = T_r^{k+1,0},$$

where index zero indicates the first order term in the Hilbert decomposition. Now, adding the three equations of (13) considered at the next order in ε leads to

$$\frac{\phi_r^{k+1,0} - \phi_r^{n,0}}{\Delta t} + \frac{1}{\beta_e^k} \frac{\phi_e^{k+1,0} - \phi_e^{n,0}}{\Delta t} + \frac{1}{\beta_i^k} \frac{\phi_i^{k+1,0} - \phi_i^{n,0}}{\Delta t} = 0,$$

which is correctly consistent with the equilibrium limit in the case of no source terms nor flux terms

$$\partial_t (E_i(T_{eq}) + E_e(T_{eq}) + E_r(T_{eq})) = 0,$$

where T_{eq} is defined by

$$T_i^0 = T_e^0 = T_r^0 = T_{eq}.$$

□

Property 6 *The numerical scheme* (20) *is steady-state-preserving.*

Proof The steady-state-preserving property is straightforward. Considering the set of Eq. (9) at equilibrium directly gives

$$\phi_e = \phi_i = \phi_r.$$

Injecting this condition in the numerical scheme (20), it is immediately observed that this state is preserved over time. □

Property 7 (Convergence of the scheme)
If Δt is small enough the sequence $(\phi^k)^{k\in\mathbb{N}} = (\phi_r, \phi_e, \phi_i)^k$ defined by (20) converges to ϕ^{n+1} solution to (9).

Proof The model studied is a differential system of the form

$$\dot{X} = A(X)X, \quad X : \mathbb{R}^N \to \mathbb{R}^N$$

where $A : \mathbb{R}^N \to \mathbb{R}^{N\times N}$ is a smooth function (of class C^1) and such that $I_N - \Delta t\, A(X)$ can be inversed for all $X \in \mathbb{R}^N$ (indeed in our case $I_N - \Delta t\, A$ is a M-matrix). The backward-Euler scheme studied writes under the form

$$\frac{X^{n+1} - X^n}{\Delta t} = A(X^{n+1})X^{n+1}, \quad X^{n+1} = (I_N - \Delta t\, A(X^{n+1}))^{-1}X^n,$$

and the corresponding implicit iterative method is

$$X^{n+1,k+1} = f_n(X^{n+1,k}), \quad f_n(X) = (I_N - \Delta t\, A(X))^{-1}X^n, \quad X^{n+1,0} = X^n.$$

Since, the scheme writes as convex combinations, if $X^n \in E$ where E is a convex bounded subset of $\mathbb{R}^N$ then

$$f_n(E) \subset E.$$

Now, using the mean value theorem (since A is regular) there exists a positive real value constant K such that

$$\forall (X_1, X_2) \in E^2, \quad ||A(X_1) - A(X_2)|| \leq K||X_1 - X_2||.$$

In addition if

$$\Delta t \max_{X\in E} ||A(X)|| < 1,$$

then

$$\forall X \in E, \quad (I_N - \Delta t\, A(X))^{-1} = I_N + \sum_{i=1}^{+\infty} (\Delta t)^i A(X)^i.$$

Consequently,

$$\forall (X_1, X_2) \in E^2, \quad ||f_n(X_1) - f_n(X_2)|| \leq \sum_{i=1}^{+\infty} (\Delta t)^i K^i ||X_1 - X_2||^i K' = \frac{\Delta t K ||X_1 - X_2|| K'}{1 - \Delta t K ||X_1 - X_2||},$$

where $K' = \max_{X\in E} ||X||$ (the above series converges if $2\Delta t K' K < 1$). Therefore there exists a positive real constant K^{max} such that

$$\forall (X_1, X_2) \in E^2, \quad ||f_n(X_1) - f_n(X_2)|| \leq \Delta t K^{max} ||X_1 - X_2||.$$

Choosing Δt such that $\Delta t K^{max} < 1$, the function f_n is a contraction mapping and the sequence $(X^{n+1,k})^{k\in\mathbf{N}}$ converges towards the unique fixed point of f_n.

□

Remark Even if the convergence result only holds under a strong CFL condition, in practice it is observed that the scheme is always convergent even working with very large time step.

4 1D Slab

The numerical strategy proposed in the previous sections is now extended in order to take into account a radiative flux under the Rosseland diffusion approximation. In the one dimensional setting a very standard three point diffusion scheme is considered for the spatial discretisation. Writing $j \in \{1, \dots, M\}$ the index of the cell the discrete radiative flux writes

$$\begin{aligned}(\partial_x F_r)_j &= \frac{F_{j+1/2} - F_{j-1/2}}{\Delta x},\\ F_{j+1/2} &= -\frac{c(\phi_{r,j+1} - \phi_{r,j})}{3\sigma_{r,j+1/2}\Delta x},\\ \sigma_{r,j+1/2} &= \sigma_R\left(\left(T_{e,j} + T_{e,j+1}\right)/2\right).\end{aligned}$$

The Euler-backward scheme becomes

$$\begin{cases}(1 + c\sigma_P^{n+1}\Delta t f^{n+1} + \dfrac{\Delta t}{\Delta x^2}(\lambda_{r,j+1/2}^{n+1} + \lambda_{r,j-1/2}^{n+1}))\phi_{r,j}^{n+1} - \dfrac{\Delta t}{\Delta x^2}(\lambda_{r,j+1/2}^{n+1}\phi_{r,j+1}^{n+1} + \lambda_{r,j-1/2}^{n+1}\phi_{r,j-1}^{n+1})\\ \qquad = \phi_{r,j}^n + c\sigma_P^{n+1}\Delta t f^{n+1}(g^{n+1}\phi_{e,j}^n + (1-g^{n+1})\phi_{i,j}^n),\\ \phi_{e,j}^{n+1} = f^{n+1}(g^{n+1}\phi_{e,j}^n + (1-g^{n+1})\phi_{i,j}^n) + (1-f^{n+1})\phi_{r,j}^{n+1},\\ \phi_{i,j}^{n+1} = h^{n+1}\phi_{i,j}^n + (1-h^{n+1})\phi_{e,j}^{n+1},\end{cases} \tag{23}$$

where f_j^{n+1}, g_j^{n+1} and h_j^{n+1} are defined in (16) and (18). The first equation of (23) can be written under the form of a linear system

$$\begin{pmatrix} d_1^{n+1} & c_1^{n+1} & & & \cdots & & 0\\ c_1^{n+1} & d_2^{n+1} & c_2^{n+1} & & & & \\ & \ddots & \ddots & \ddots & & & \vdots\\ & & c_{j-1}^{n+1} & d_j^{n+1} & c_j^{n+1} & & \\ \vdots & & & \ddots & \ddots & \ddots & \\ & & & & c_{M-2}^{n+1} & d_{M-1}^{n+1} & c_{M-1}^{n+1}\\ 0 & & \cdots & & & c_{M-1}^{n+1} & d_M^{n+1}\end{pmatrix}\begin{pmatrix}\phi_{r,1}^{n+1}\\ \\ \vdots\\ \phi_{r,j}^{n+1}\\ \vdots\\ \\ \phi_{r,M}^{n+1}\end{pmatrix} = \begin{pmatrix} b_1^{n+1}\\ \\ \vdots\\ b_j^{n+1}\\ \vdots\\ \\ b_M^{n+1}\end{pmatrix}, \tag{24}$$

where

$$\begin{aligned} c_j^{n+1} &= -\frac{\Delta t}{\Delta x^2}\lambda_{r,j+1/2}^{n+1}, \qquad \lambda_{r,j+1/2}^n = \frac{c}{3\sigma_{r,j+1/2}^n},\\ b_j^{n+1} &= \phi_{r,j}^n + c\sigma_P^{n+1}\Delta t f^{n+1}(g^{n+1}\phi_{e,j}^n + (1-g^{n+1})\phi_{i,j}^n),\\ d_j^{n+1} &= 1 + c\sigma_P^{n+1}\Delta t f^{n+1} + \frac{\Delta t}{\Delta x^2}(\lambda_{r,j+1/2}^{n+1} + \lambda_{r,j-1/2}^{n+1}).\end{aligned}$$

We denote A^{n+1} the matrix of the system and write $A^{n+1} = D^{n+1} + E^{n+1} + F^{n+1}$ where D^{n+1} contains the diagonal of A^{n+1}, E^{n+1} the lower triangular part and F^{n+1} the upper

triangular part. System (24) can be written

$$(D^{n+1}+E^{n+1}+F^{n+1})\Phi^{n+1}=B^{n+1},\quad \Phi^{n+1}=\begin{pmatrix}\phi_{r,1}^{n+1}\\ \vdots\\ \phi_{r,j}^{n+1}\\ \vdots\\ \phi_{r,M}^{n+1}\end{pmatrix},\quad B^{n+1}=\begin{pmatrix}b_1^{n+1}\\ \vdots\\ b_j^{n+1}\\ \vdots\\ b_M^{n+1}\end{pmatrix}.$$

Remark Similarly to the quantities σ_P and κ, σ_R can be chosen implicit or explicit (see "Appendix 1").

4.1 Implicit Iterative Strategies

While the spatial discretisation is straightforward, in this part, different time discretisation strategies are presented and compared.

4.1.1 Jacobi Procedure

The first temporal discretisation considered lies on a local iterative implicit procedure. Here, only the diagonal terms are chosen implicit and the linear system (24) writes

$$D^{n+1,k}\Phi^{n+1,k+1}=B^{n+1,k}-(E^{n+1,k}+F^{n+1,k})\Phi^{n+1,k}.$$

The last equation of (23) becomes

$$\begin{cases}\phi_{e,j}^{n+1,k+1}=f_j^k(g_j^k\phi_{e,j}^n+(1-g_j^k)\phi_{i,j}^n)+(1-f_j^k)\phi_{r,j}^{n+1,k+1},\\ \phi_{i,j}^{n+1,k+1}=h_j^k\phi_{i,j}^n+(1-h_j^k)\phi_{e,j}^{n+1,k+1}.\end{cases}\tag{25}$$

In the following this numerical scheme is called the Jacobi method.

4.1.2 Gauss–Seidel Procedure

In this section the temporal discretisation of the radiative flux uses the quantities already computed at time t^{n+1} to improve the convergence of the method. In addition, in order to increase the convergence speed we choose, at each sub-iteration k, to switch between a direct method and a retrograde method. More precisely the implicit scheme (24) is solved by

$$\begin{aligned}(D^{n+1,k}+E^{n+1,k})\Phi^{n+1,k+1}&=B^{n+1,k}-F^{n+1,k}\Phi^{n+1,k} &&\text{if k is even,}\\ (D^{n+1,k}+F^{n+1,k})\Phi^{n+1,k+1}&=B^{n+1,k}-E^{n+1,k}\Phi^{n+1,k} &&\text{if k is odd.}\end{aligned}$$

The last equations of (23) still write as (25). This iterative method is called the Gauss–Seidel method in the following.

4.1.3 Conjugate Gradient Procedure

Here, all the terms in the discretisation of the radiative flux are considered implicit so the resolution of an linear system at each sub-iteration k is required. This is done by a standard conjugate gradient method. In this case, the iterative method of the implicit scheme reads

$$(D^{n+1,k} + E^{n+1,k} + F^{n+1,k})\Phi^{n+1,k+1} = A^{n+1,k}\Phi^{n+1,k+1} = B^{n+1,k},$$

and the other equations of the scheme writes as (25). In the following this numerical method is called the conjugate gradient method.

4.1.4 Hybrid Methods

In the following section it will shown that the convergence of the Jacobi and the Gauss–Seidel methods is slow compared to the one of the conjugate gradient method. However, it is possible to combine these methods to obtain very fast and stable algorithms. More precisely, the idea is to start by using the conjugate gradient method in the first iterations (let us call N this iteration number) then use the Jacobi or the Gauss–Seidel method. These two methods are called the hybrid Jacobi method and the hybrid Gauss–Seidel method. The influence of the iteration number before switching to a method to another is discussed in the next section.

Remark Of course, it is possible to start a simulation using the Jacobi or the Gauss–Seidel method then work with the conjugate gradient method.

4.2 Numerical Properties

The numerical properties established for the ODE system are now extended to the PDE system.

Property 8 *The Jacobi, Gauss–Seidel the conjugate gradient schemes conserve the discrete total energy.*

Proof With Property 3 (energy conservation in 0D), the energy conservation property for the PDE model is straightforward. For the three strategies (Jacobi, Gauss–Seidel and conjugate gradient) the radiative diffusion term is conservative at convergence. The scheme obtained is conservative and correctly consistent with the energy conservation law (5). The total energy in the domain is then conserved. □

Property 9 *The Jacobi, the Gauss–Seidel and conjugate gradient scheme are asymptotic-preserving in the limit $c\sigma_P$ and $c\kappa$ tend to infinity.*

Proof The proof is similar to the proof provided in the 0D case. Let τ be the characteristic time of evolution and ε the dimensionless quantity

$$\varepsilon = 1/\max(c\sigma_P\tau, c\kappa\tau).$$

Scaling the three schemes with τ and letting ε tend to zero gives at the first order in ε (terms similar to the 0D case)

$$\phi_i^{k+1,0} = \phi_e^{k+1,0} = \phi_r^{k+1,0},$$

which by definition of ϕ_α is equivalent to

$$T_i^{k+1,0} = T_e^{k+1,0} = T_r^{k+1,0},$$

where index zero indicates the first order term in the Hilbert decomposition. Now, adding the three equations of (14) considered at the next order in ε leads to (in the case of the Jacobi scheme)

$$\frac{\phi_r^{k+1,0}-\phi_r^{n,0}}{\Delta t}+\frac{1}{\beta_e^k}\frac{\phi_e^{k+1,0}-\phi_e^{n,0}}{\Delta t}+\frac{1}{\beta_i^k}\frac{\phi_i^{k+1,0}-\phi_i^{n,0}}{\Delta t}$$
$$=\frac{\lambda^n_{r,j+1/2}(\phi^{k,0}_{r,j+1}-\phi^{k+1,0}_{r,j})-\lambda^n_{r,j-1/2}(\phi^{k+1,0}_{r,j}-\phi^{k,0}_{r,j-1})}{\Delta x^2},$$

which is correctly consistent with the equilibrium limit (in the case of no source terms)

$$\partial_t(E_i(T_{eq})+E_e(T_{eq})+E_r(T_{eq}))+\nabla.F_r(T_{eq})=0,$$

where T_{eq} is defined by

$$T_i^0=T_e^0=T_r^0=T_{eq}.$$

The procedure is the same for the Gauss–Seidel and conjugate-gradient schemes. □

Property 10 *The Jacobi and Gauss–Seidel scheme are unconditionally L^∞ stable. The conjugate-gradient scheme is unconditionally positive.*

Proof The L^∞ stability property of the Jacobi and Gauss–Seidel scheme is simply established by writing them under the form of convex combinations. Unfortunately, the conjugate gradient method does not write under this formalism. However, the associated matrix given in (24) is a M-matrix and the components of vector b are positive (convex combination of positive terms), therefore the solution remains positive. □

Drawbacks of standard higher-order time extensions

It is possible and easy to construct second-order (or high-order) implicit schemes based on standard implicit Runge–Kutta strategies. However, while it is possible to use explicit Runge–Kutta schemes based on convex-combinations to ensure the L^∞ stability property, it is not the case with implicit Runge–Kutta. Therefore, one understands the difficulty in getting high-order schemes while enforcing the L^∞ property and dealing with the stiffness. To illustrate this we consider the very simple toy ordinary differential equation

$$y'(t)=-y(t)/\varepsilon,$$

where ε is a small parameter. The backward-Euler scheme reads

$$y^{n+1}=\frac{\varepsilon}{\varepsilon+\Delta t}y^n,$$

which is obviously unconditionally stable and asymptotic-preserving (for a fixed Δt, in the limit ε tends to zero, the limit scheme is $y^{n+1}=0$ which is consistent with the limit model $y(t)=0$). Now consider a standard implicit second-order Runge–Kutta scheme associated to the following Butcher tableau

$$\begin{array}{c|cc} 0 & 0 & \\ 1 & \frac{1}{2} & \frac{1}{2} \\ \hline & \frac{1}{2} & \frac{1}{2} \end{array}$$

leads in this simple linear case to

$$y^{n+1}=\frac{2\varepsilon-\Delta t}{2\varepsilon+\Delta t}y^n. \tag{26}$$

Even if this scheme is A-stable the positivity of the solution is only ensured if the time time step Δt remains smaller than 2ε which of course is prohibitive. The same issue arises with the three temperature model studied here. In this case, the second order implicit Runge–Kutta scheme reads

$$\phi^{n+1} = \phi^n + \frac{\Delta t}{2} A(\phi^n)\phi^n + \frac{\Delta t}{2} A(\phi^{n+1})\phi^{n+1},$$

with

$$\phi^n + \frac{\Delta t}{2} A(\phi^n)\phi^n = \begin{pmatrix} \phi_r^n + \frac{1}{2} c\Delta t \sigma_P (\phi_e^n - \phi_r^n) \\ \phi_e^n + \frac{1}{2} c\Delta t \sigma_P \beta_e^n (\phi_r^n - \phi_e^n) + c\Delta t \frac{1}{2} \kappa^n \beta_e^n \delta_{ie}^n (\phi_i^n - \phi_e^n) \\ \phi_i^n + \frac{1}{2} c\Delta t \kappa^n \beta_i^n \delta_{ie}^n (\phi_e^n - \phi_i^n) \end{pmatrix}. \quad (27)$$

While it is possible to show that the matrix $[I_3 - \frac{\Delta t}{2} A(\phi^{n+1})]^{-1}$ is a stochastic matrix, unfortunately the coefficients of $\phi^n + \frac{\Delta t}{2} A(\phi^n)\phi^n$ may be negative. This phenomena may for example occur when the electronic temperature is much larger than the ionic and radiative temperatures (see problem 3 in the numerical results section). Indeed, in this case, the second component of Eq. (27) is negative (if σ_P and κ are large enough).

One may think, in the spirit of MOOD strategies, in using standard high order implicit Runge–Kutta schemes and detect at posteriori if the L^∞ property is satisfied. If it is not the case, the solution is recomputed (only in the stencil) with a lower order Runge–Kutta scheme. This process is repeated until the first order implicit scheme (which is L^∞ stable) is reached if necessary. However, for the kind of applications we are interested in, the strong stiffness of the problem directly leads us to use the first order scheme.

In addition, even if a high-order implicit L^∞ stable scheme was available, the asymptotic-preserving property is mandatory here. In particular the second-order implicit Runge–Kutta scheme (26) does not keep the asymptotic-preserving property even for the simple toy model.

Finally, the extension to higher-order schemes while keeping both the asymptotic-preserving property and the L^∞ stability property seems particularly challenging even in the 0D case. It is maybe possible to derive high-order schemes by releasing one of these properties (for example retaining only the positivity instead of the L^∞ stability) but even this is not straightforward and should be investigated in details. For these reasons and the kind of applications we are interested in, we believe the implicit first order scheme presented in this communication should be preferred instead of standard high-order implicit schemes (which are not L^∞ stable nor asymptotic-preserving for large Δt).

5 Electronic and Ionic Conductivities

The contribution of the electronic and the ionic conductivities are now included. It is shown that the reformulation procedure and the numerical strategy of the previous sections can be naturally extended.

5.1 Model and Numerical Strategy

Spitzer–Härm formulae [14] are considered for electronic and ionic conductivities so that in the one dimensional framework the system studied reads

$$\begin{cases} \partial_t E_r + \partial_x(\lambda_r \partial_x E_r) = c\sigma_P(aT_e{}^4 - E_r), \\ \partial_t E_e + \partial_x(\lambda_e^{'} \partial_x E_e) = c\sigma_P(E_r - aT_e{}^4) + c\kappa(T_i - T_e), \\ \partial_t E_i + \partial_x(\lambda_i^{'} \partial_x E_i) = c\kappa(T_e - T_i), \end{cases} \tag{28}$$

where the radiative, electronic and ionic conductivities are defined in (3). Now, following the same procedure as in the first section, model (28) is rewritten as

$$\begin{cases} \partial_t \phi_r + \partial_x(\lambda_r \partial_x \phi_r) = c\sigma_P(\phi_e - \phi_r), \\ \partial_t \phi_e + \beta_e \partial_x(\lambda_e \partial_x \phi_e) = \beta_e c\sigma_P(\phi_r - \phi_e) + \beta_e c\kappa\delta_{ie}(\phi_i - \phi_e), \\ \partial_t \phi_i + \beta_i \partial_x(\lambda_i \partial_x \phi_i) = \beta_i c\kappa\delta_{ie}(\phi_e - \phi_i), \end{cases} \tag{29}$$

where

$$\lambda_e = \frac{1}{\beta_e}\lambda_e^{'}, \qquad \lambda_i = \frac{1}{\beta_i}\lambda_i^{'}.$$

The model is now well-suited to apply the numerical strategy presented in the previous sections.

5.2 Numerical Properties

The numerical properties established in the previous sections naturally extend to the full model (28).

Property 11 *The Jacobi, Gauss–Seidel and conjugate gradient schemes apply to the set of Eq. (29) conserve the discrete total energy.*

Proof Using Property 3 (energy conservation in 0D), the energy conservation property is straightforward. For the three strategies (Jacobi, Gauss–Seidel and conjugate gradient) the radiative diffusion, the electronic and ionic conductivities terms are conservative at convergence. Adding the three equations the resulting scheme obtained is conservative and correctly consistent with the energy conservation law (5). □

Property 12 *The Jacobi, the Gauss–Seidel and conjugate gradient scheme are asymptotic-preserving in the limit σ_P and $c\kappa$ tend to infinity.*

Proof The proof is similar to the proof provided in the previous section. By considering the scaling and the Hilbert expansion procedure give by adding the three equations (in the case of the Jacobi scheme)

$$\begin{aligned} &\frac{\phi_{r,j}^{k+1,0} - \phi_{r,j}^{n,0}}{\Delta t} + \frac{1}{\beta_e^k}\frac{\phi_{e,j}^{k+1,0} - \phi_{e,j}^{n,0}}{\Delta t} + \frac{1}{\beta_i^k}\frac{\phi_{i,j}^{k+1,0} - \phi_{i,j}^{n,0}}{\Delta t} \\ &= \frac{\lambda_{r,j+1/2}^k(\phi_{r,j+1}^{k,0} - \phi_{r,j}^{k+1,0}) - \lambda_{r,j-1/2}^k(\phi_{r,j}^{k+1,0} - \phi_{r,j-1}^{k,0})}{\Delta x^2} \\ &\quad + \frac{\lambda_{e,j+1/2}^{k,0}(\phi_{e,j+1}^{k,0} - \phi_{e,j}^{k+1,0}) - \lambda_{e,j-1/2}^{k,0}(\phi_{e,j}^{k+1,0} - \phi_{e,j-1}^{k,0})}{\Delta x^2} \\ &\quad + \frac{\lambda_{i,j+1/2}^{k,0}(\phi_{i,j+1}^{k,0} - \phi_{i,j}^{k+1,0}) - \lambda_{i,j-1/2}^{k,0}(\phi_{i,j}^{k+1,0} - \phi_{i,j-1}^{k,0})}{\Delta x^2}. \end{aligned}$$

which is correctly consistent with the equilibrium limit (in the case of no source terms)

$$\partial_t(E_i(T_{eq}) + E_e(T_{eq}) + E_r(T_{eq})) + \nabla.(F_r(T_{eq}) + F_e(T_{eq}) + F_i(T_{eq})) = 0,$$

where T_{eq} is defined by

$$T_i^0 = T_e^0 = T_r^0 = T_{eq}.$$

The procedure is the same for the Gauss–Seidel and conjugate-gradient schemes. □

Property 13 *The Jacobi and Gauss–Seidel scheme are unconditionally L^∞ stable. The conjugate-gradient scheme is unconditionally positive.*

Proof The L^∞ stability property of the Jacobi and Gauss–Seidel scheme is shown by writing them under the form of convex combinations. In the case of the Jacobi method the procedure is the following. Firstly using the ionic energy equation $\phi_{i,j}^{k+1}$ is written as convex combinations of $\phi_{i,j}^n$, $\phi_{e,j}^{k+1}$, $\phi_{i,j+1}^k$ and $\phi_{i,j-1}^k$. Then, using the electronic energy equation and the relation just obtained $\phi_{e,j}^{k+1}$ is written as convex combinations of $\phi_{e,j}^n$, $\phi_{r,j}^{k+1}$, $\phi_{i,j+1}^k$, $\phi_{i,j-1}^k$, $\phi_{e,j+1}^k$ and $\phi_{e,j-1}^k$. Finally, this last relation is combined with the radiation energy equation to write $\phi_{r,j}^{k+1}$ as convex combinations of $\phi_{r,j}^n$, $\phi_{r,j+1}^{k+1}$, $\phi_{r,j-1}^{k+1}$, $\phi_{i,j+1}^k$, $\phi_{i,j-1}^k$, $\phi_{e,j+1}^k$ and $\phi_{e,j-1}^k$. The procedure is the same for the Gauss–Seidel scheme. Unfortunately similarly to the previous section the conjugate gradient method does not write under this formalism (no convex combinations). However, the matrix associated to the resulting linear system is a M-matrix and the components of the right-hand side vector are positive, therefore the solution remains positive. □

6 Numerical Test Cases

6.1 Numerical Results in 0D Settings (No Spatial Variation)

The two first test cases we consider are taken from [3]. At initial time the three temperatures are set equal. External source terms are applied and the separation of the temperature profiles is studied.

Problem 1 and 2. The values of the physical parameters and the initial quantities are given in Table 1. The external source term appears on the ions equation and writes

$$\int_{t_1}^{t_2} Q_i(t)\mathrm{d}t = \frac{A}{2}\left(\mathrm{erf}\left(\frac{t_2 - t_c}{\sqrt{2}t_w}\right) - \mathrm{erf}\left(\frac{t_1 - t_c}{\sqrt{2}t_w}\right)\right), \tag{30}$$

where

$$A = 75.19884, \qquad t_c = 10, \qquad t_w = 1,$$

and erf is the standard error function. In order to explain how to use expression (30) we consider a simplified form of the last equation of (9) (it works the same for the general model and the scheme presented here)

$$\partial_t \phi_i = \beta_i Q_i.$$

Integrating in time between $[t^n, t^{n+1}]$ this equation gives

$$\phi_i(t^{n+1}) - \phi_i(t^n) = \int_{t^n}^{t^{n+1}} \beta_i(t) Q_i(t) dt \approx \beta_i(t^{n+1}) \int_{t^n}^{t^{n+1}} Q_i(t) dt.$$

Now the last integral in the previous equation is exactly given by expression (26) therefore the scheme writes

$$\phi_i^{n+1} - \phi_i^n = \beta_i^{n+1} \int_{t^n}^{t^{n+1}} Q_i(t) dt = \beta_i^{n+1} \frac{A}{2}\left(\mathrm{erf}\left(\frac{t^{n+1} - t_c}{\sqrt{2}t_w}\right) - \mathrm{erf}\left(\frac{t^n - t_c}{\sqrt{2}t_w}\right)\right).$$

Table 1 Parameters and initial quantities used for Problem 1 and 2

	Problem 1	Problem 2
c	29.979	29.979
a	0.01372	0.01372
σ_p	$0.5 \times T_e^{-2}$	$0.1 \times T_e^{-2}$
κ	0.1	$0.01379 \times (T_e)^{-1/2}$
$\rho C_{v,i}$	0.15	0.15
$\rho C_{v,e}$	0.3	$0.3 \times T_e$
$T_i = T_e = T_r$	2.52487×10^{-5}	2.52487×10^{-5}
A	75.19884	15.03978

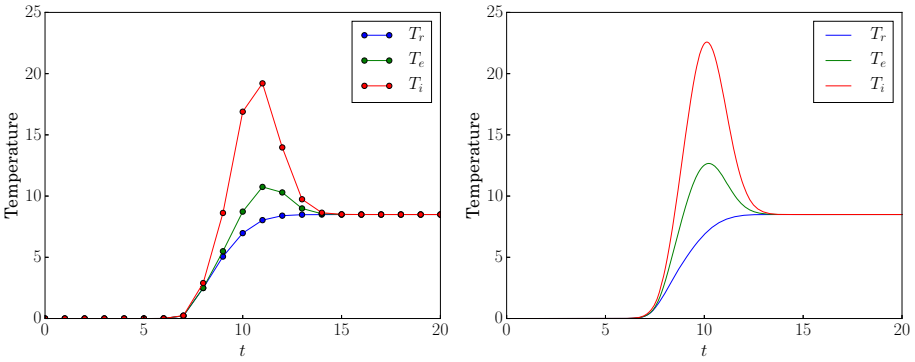

Fig. 1 Problem 1. Time evolution of the three temperature profiles using a large time step (left) and a smaller time step (right)

Figures 1 and 2 display the time evolution of temperatures obtained with the scheme (22) for Problem 1 and Problem 2. For small time steps (Figs. 1b and 2b) one recovers the results found in [3]. In addition, it is observed that even using very large time steps (Figures 1a and 2a) the scheme (22) produces sensible numerical solutions. In the two numerical test cases considered in [3], the quantity ϕ_i^n remains larger than ϕ_e^n. We propose here, a slight modification of Problems 1 and Problem 2 to check configurations where it is not the case.

Problem 3. This test case reconsiders the data of the Problem 1 but the three temperatures are not initially equal (see Table 2).

Problem 4. This test case use the data of Problem 2 but the ionic energy source (30) is replaced by a radiative energy source of the same value

$$\int_{t_1}^{t_2} Q_r(t)\mathrm{d}t = \frac{A}{2}\left(\mathrm{erf}\left(\frac{t_2 - t_c}{\sqrt{2}t_w}\right) - \mathrm{erf}\left(\frac{t_1 - t_c}{\sqrt{2}t_w}\right)\right).$$

In Figs. 3 and 4 it is shown that the scheme (22) give reasonable results for the Problem 3 and Problem 4 even working with very large time step (see Figs. 9a and 4a). We mention here that these configurations are problematic for the scheme proposed in [3] in which negative temperatures can be obtained. In our case, thanks to the strong stability property (unconditionally L^∞ stability) this can not occur even for very large time steps.

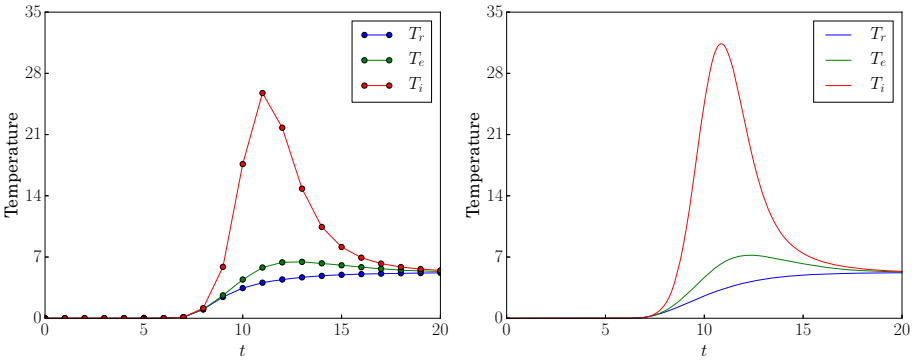

(a) $\Delta t = 1ns$ **(b)** $\Delta t = 0.001ns$

Fig. 2 Problem 2. Time evolution of the three temperature profiles using a large time step (left) and a smaller time step (right) obtained with nonlinear $\rho C_{v,e}$ and κ

Table 2 Parameters and initial quantities used for Problem 3 and 4

	Problem 3	Problem 4
c	29.979	29.979
a	0.01372	0.01372
σ_p	$0.5 \times T_e^{-2}$	$0.1 \times T_e^{-2}$
κ	0.1	$0.01379 \times (T_e)^{-1/2}$
$\rho C_{v,i}$	0.15	0.15
$\rho C_{v,e}$	0.3	$0.3 \times T_e$
T_i	2.52487×10^{-1}	2.52487×10^{-5}
T_e	2.52487×10^{1}	2.52487×10^{-5}
T_r	2.52487×10^{-1}	2.52487×10^{-5}
A	75.19884	15.03978

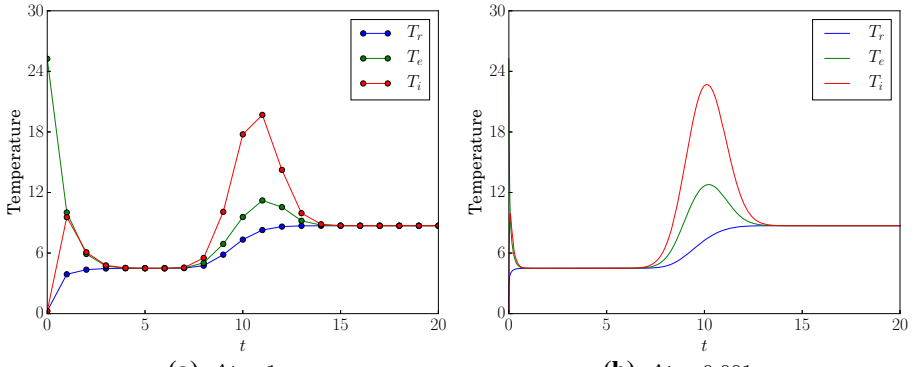

(a) $\Delta t = 1ns$ **(b)** $\Delta t = 0.001ns$

Fig. 3 Problem 3. Time evolution of the three temperature profiles using a large time step (left) and a smaller time step (right)

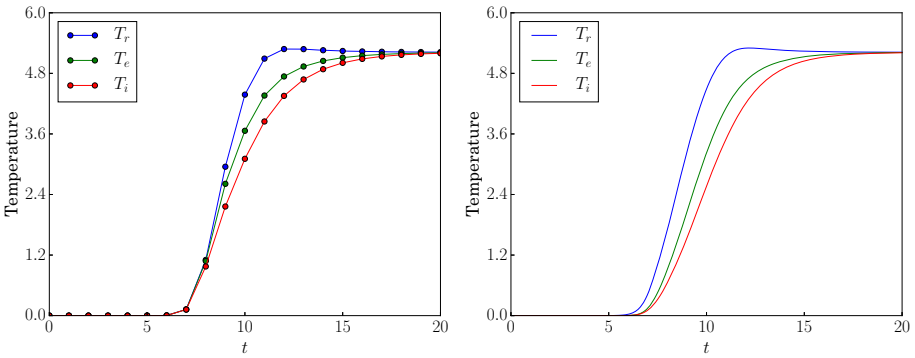

Fig. 4 Problem 4. Time evolution of the three temperature profiles using a large time step (left) and a smaller time step (right)

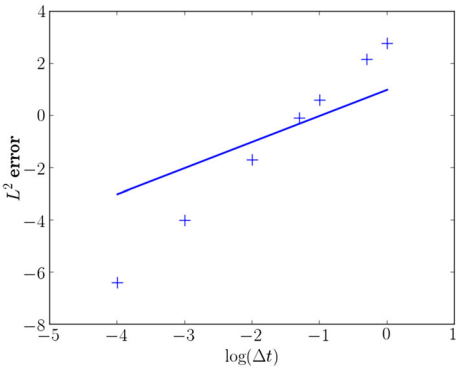

Fig. 5 L^2 error for different time step Δt. The slope of the straight line in blue is 1

Numerical convergence in 0D

We check the accuracy on the scheme in this 0D setting by comparing the results with reference solutions [2,3]. In Fig. 5 the error between the numerical solution and a reference solution is displayed for different time steps for Problem 1. Similar results are obtained for Problems 2, 3 and 4. It is observed that the scheme is correctly convergent. More precisely, the slope of the strait line in blue is 1, therefore it is observed that the coonvergence in time of the scheme is correctly of order one. For this test case, the accuraccy seems more than one but since the temporal discretisation is first order accurate [see discussion in Sect. (4.2)] we believe this extra-convergence is not relevant. In the 1D case it is observed the scheme is first order.

6.2 Numerical Results in the 1D Slab

6.2.1 Asymptotic Behavior

The asymptotic-preserving property of the scheme is now investigated. In the limit $c\sigma$ and $c\kappa$ tend to infinity, it is expected the three temperatures to be equal and exhibit a diffusion equation behavior. For this purpose we study the relaxation of an initial energy profile for

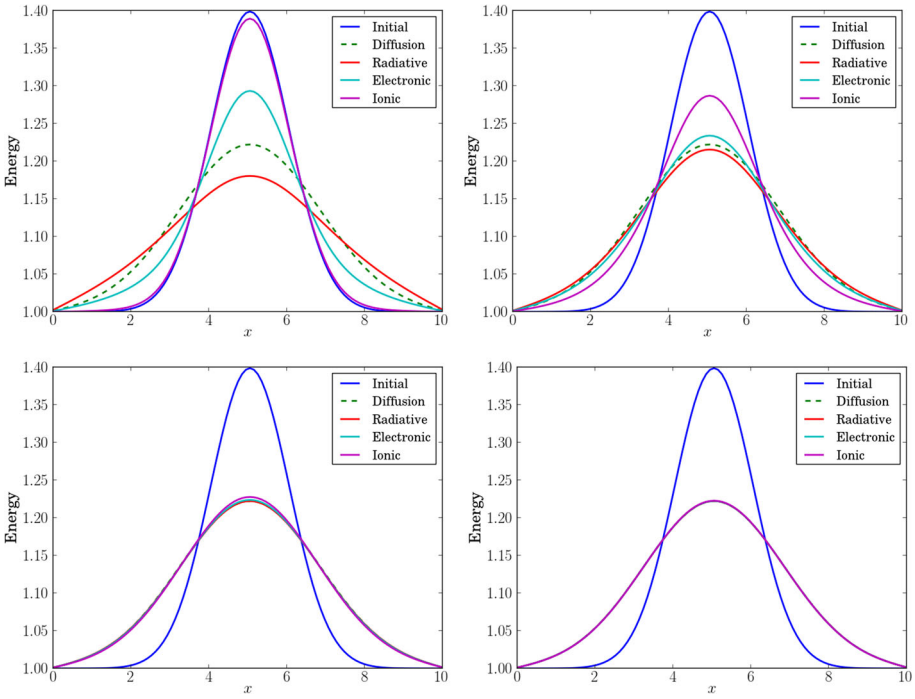

Fig. 6 Energy profiles obtained for different values of $c\sigma = c\kappa$. The results are displayed for $c\sigma = c\kappa = 10^{-1}$ (top left), $c\sigma = c\kappa = 10^{0}$ (top right), $c\sigma = c\kappa = 10^{1}$ (bottom left) and $c\sigma = c\kappa = 10^{2}$ (bottom right). In the limit $c\sigma$ and $c\kappa$ tend to infinity the diffusion limit is correctly recovered

different values of $c\sigma$ and $c\kappa$ of the form

$$\phi_e = \phi_i = \phi_r = 1 + \exp(-0.5(x-5)^2)/\sqrt{2\pi},$$

where the space domain is [0, 10] and we have set $\Delta x = 0.1$, $\Delta t = 10^{-3}$, $\rho C_{v,\alpha} = 4aT_\alpha^3$, $a = c = \sigma_R = 1$ and $c\sigma_P = c\kappa$. The final time is $t = 10$. In Fig. 6, the three energy profiles obtained for different values of $c\sigma_P = c\kappa$ are displayed. The results are shown for $c\sigma_P = c\kappa = 10^{-1}$ (top left), $c\sigma_P = \kappa = 10^{0}$ (top right), $c\sigma_P = c\kappa = 10^{1}$ (bottom left) and $c\sigma_P = c\kappa = 10^{2}$ (bottom right). In addition the solutions of a direct discretisation of the limit diffusion equation is displayed in dashed green. It is observed that for small values of $c\sigma_P = c\kappa$, the three temperature profiles are very different while they become closer as $c\sigma_P = c\kappa$ increases. As expected, for large values $c\sigma_P = c\kappa$ (for example larger than 10^2), the electronic, ionic and radiative energy profiles correctly match with the diffusion solution. The correct asymptotic behavior is then recovered.

Numerical convergence in 1D

We now check the accuracy of the scheme in 1D for this test case. In Fig. 7 the L^∞ error between the numerical solution and a converged solution (obtained with a very refined mesh) is displayed for different space steps. It is observed that the scheme is correctly convergent. More precisely, the slope of the strait line in blue is 2, therefore the scheme is correctly second order accurate in space (standard discretisation of a diffusion operator). A similar convergence analysis in time shows that the scheme is first order accurate in time.

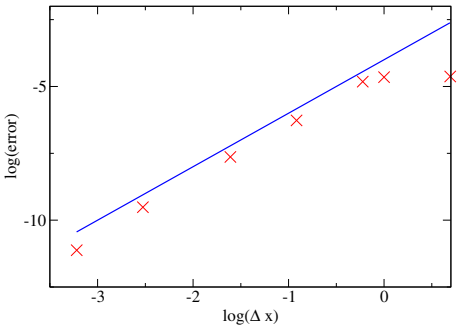

Fig. 7 L^{∞} error for different space step Δx. The slope of the straight line in blue is 2. The scheme is correctly second order accurate in space (Color figure online)

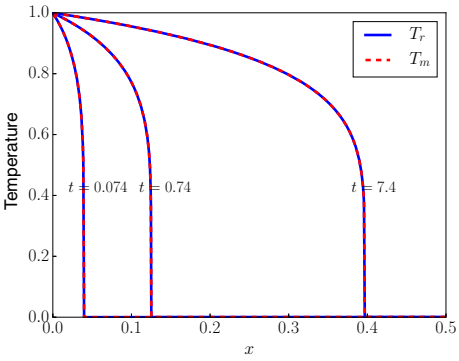

Fig. 8 Test case Marshak2A. Temperature profile using 1000 cells and a time step of $\Delta t = 1 \times 10^{-3}$ sh at different times

6.2.2 Marshak2A Test Case

The numerical test case we consider consists in the propagation of a Marshak wave and is taken from [15]. In the following we refer to it as the Marshak2A test case. The space interval is $[0, 0.5]$ and the physical constant are $c = 299.79$ and $a = 0.01372$. The coefficient κ is taken sufficiently large to ensure $T_e = T_i = T_m$. We consider $\rho C_{v,e} = 0.03$ and $\rho C_{v,i} = 0.27$. The absorption opacity and the Rosseland opacity follow the relation $\sigma_P = \sigma_R = 300 T_m^{-3}$. At initial time, all the temperatures are set equal with $T_r = T_m = 1 \times 10^{-6}$. Concerning the boundary condition, a temperature of $T_e = T_i = T_r = 1$ at the left boundary while a Neumann outgoing flux condition is considered in $x = 0.5$. The temperature profile obtained is displayed on Fig. 8 for different times.

In practice it is observed that all the numerical schemes (Jacobi, Gauss–Seidel, conjugate gradient and hybrid) recover the same correct temperature profiles. At convergence, the others numerical scheme presented in the previous sections give the same results. However, it is observed that the computational time required by the different schemes is greatly different.

Importance of the energy conservation

In this section the conservative scheme presented in this communication is compared with the same scheme for which another definition of the parameter β_α is considered. For this news scheme, instead of choosing the definition (11), we consider $\beta_\alpha = (4aT_\alpha^3)/(\rho C_{v,\alpha})$ (see Eq. 7). By definition of β_α this scheme is correctly consistent but is not exactly conservative. The two schemes are compared with a reference solution in Fig. 9. As expected, it is observed that for a given mesh the conservative scheme presented is the most accurate. This demonstrates the importance of the energy conservation property.

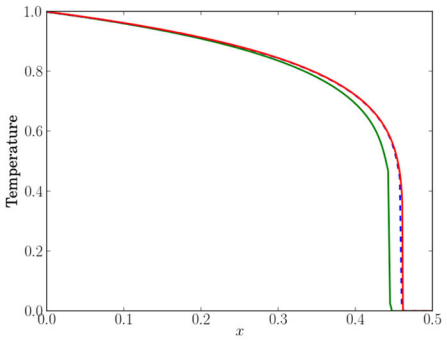

(a) Temporal profiles displayed for the conservative scheme in blue and the non-conservative scheme is green. The reference solution is in red.

(b) Temporal evolution of the total energy in the domain. The reference is in red, the conservative scheme in blue and the non-conservative scheme is green.

Fig. 9 Influence of the energy conservation

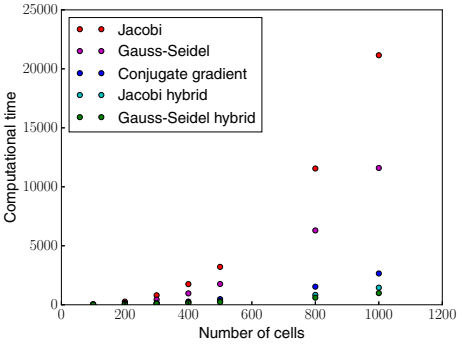

Fig. 10 Computational time in term of the cell number for $\Delta t = 1 \times 10^{-3}$

Computational times

The computational time of the different methods is computed in terms of the mesh number keeping the same time step $\Delta t = 1 \times 10^{-3}$. Since the computational time of the hybrid method depends on the parameter N (number of iterations before switching from one method to another) we choose the optimal number N. Figure 10 shows that the convergence of the Jacobi method is slow compared to the other numerical methods. The Gauss–Seidel method is much faster but remains slow compared to the conjugate gradient method. Indeed, even if a linear system is solved at each sub-step k it is observed that the converge is very fast. Finally, it is shown that by using the optimal number of iteration N that hybrid methods can become faster than the conjugate gradient method.

Hybrid methods

As mentioned in the previous section, the convergence speeds of the hybrid methods strongly depend on the iteration number N (number of iteration of a first method before working with a second). Unfortunately, it is observed that the optimal iteration number N depends on the test case considered but also on the time step and space step used. In Fig. 11 the computational time is displayed as function of N for different meshes keeping $\Delta t = 1 \times 10^{-3}$. It is observed that hybrid methods are often faster than the gradient conjugate method. However, it does not seem easy to have access to the optimal iteration number before running a simulation.

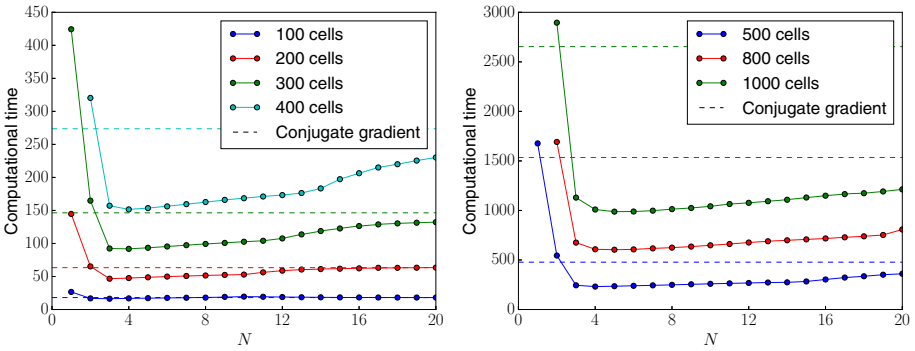

(a) 100 to 400 cells **(b)** 500 to 1000 cells

Fig. 11 Computational time as function of N (number of sub-iterations using the gradient conjugate method before switching to the Gauss–Seidel method) for different meshes

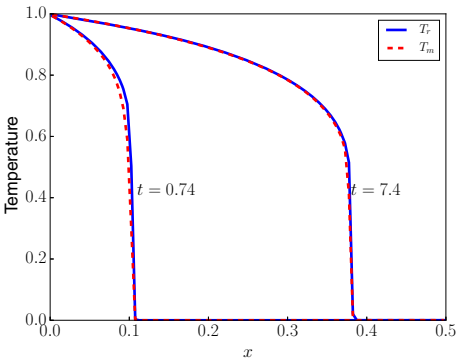

Fig. 12 Modified Marshak2A test case. Temperature profiles using 500 cells for different times

That is why, this parameter can be left to the user. We mention here that by default the user may consider the gradient conjugate method which is already very fast.

6.2.3 Modified Marshak2A

First modifications

For this test case, the numerical test case Marshak2A of the previous section is modified such as the radiative temperature T_r and the matter temperature T_m do not remain equal. The Rosseland opacity remains $\sigma_R = 300T_m^{-3}$ but the absorption opacity is changed to $\sigma_P = \sigma_R/100 = 3T_m^{-3}$. The parameter κ is kept sufficiently large to enforce $T_e = T_i = T_m$. The numerical results obtained are displayed in Fig. 12. As expected, one observes slight differences between the two temperatures profiles $T_e = T_i = T_m$ and T_r.

Second modifications

In order to observe the decoupling of the electronic and ionic temperatures T_e and T_i, several values of the parameter κ are considered. In Fig. 13 different temperature profiles are displayed for various values of κ.

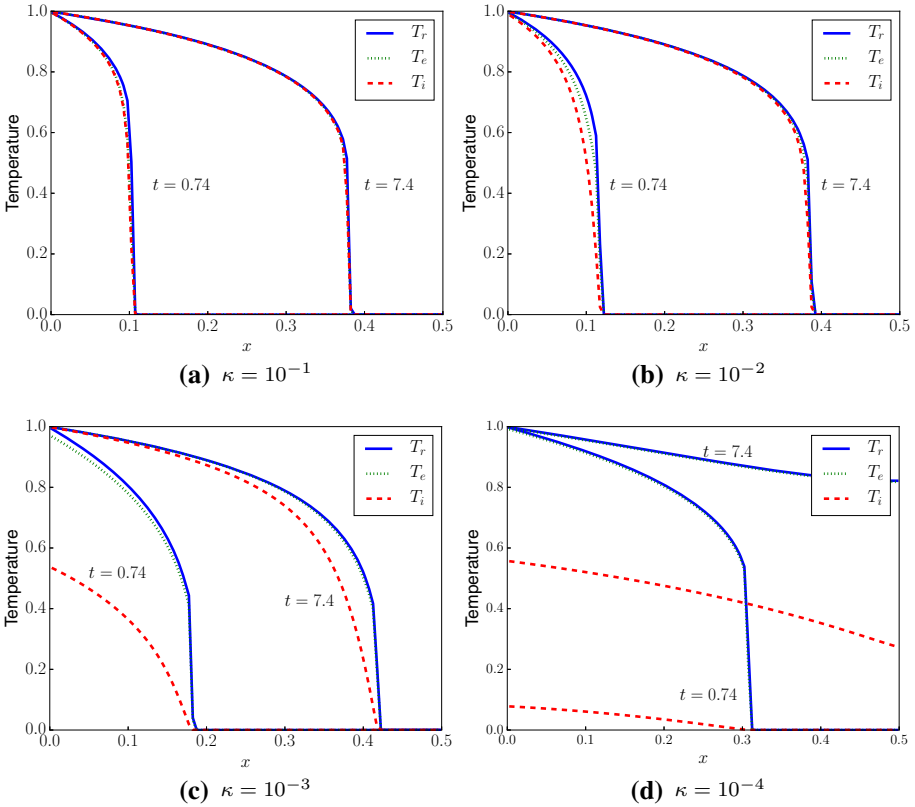

Fig. 13 Modified Marshak2A test case. Representation of the temperature profiles for different values of κ at different times

6.2.4 Electronic and Ionic Conductivities

The Marshak2A test case is reconsidered taking into account the electronic and ionic conductivities (Spitzer formalism). We set $\lambda_e^{'} = K$, $\lambda_i^{'} = K/100$ and study the temperature profiles for different values of the parameter K. The results are displayed in Fig. 14. As expected, in the case $K = 0$, the results of the Marshak2A test case are recovered. Then, as the parameter K increases (so the electronic and ionic conductivities), one notices that the temperature profiles spread out more rapidly.

Conclusion

Robust and accurate numerical schemes have been proposed and analyzed for solving a three temperature plasma model. Thanks to an appropriate recast of the model, convex combination-based numerical schemes with strong stability properties can be derived. Discrete energy conservation and asymptotic-preserving properties are also proved and the numerical results are found to be close to the ones obtained in [3].

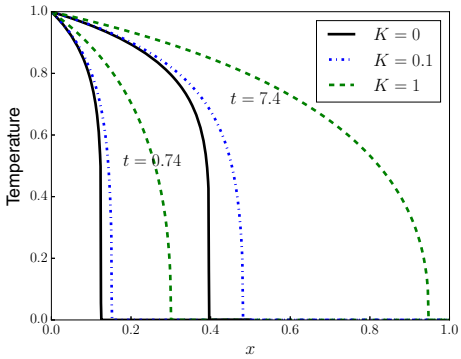

Fig. 14 Marshak2A test case with electronic and ionic conductivities for three different values of K at time $t = 0.74$ (right) and time $t = 7.4$ (left)

The method has then been extended to include radiative fluxes. Different implicit iterative time discretisations have been proposed and compared. It has been observed that the conjugate gradient method is much faster than the Jacobi and the Gauss–Seidel methods. We also noticed that hybrid methods may enable even faster simulations. Finally, the numerical strategy has been extended to include the contributions of the electronic and ionic conductivities.

A natural perspective deals with the extension to several space dimensions on cartesian and non-structured meshes. We believe the methodology proposed here can be extended easily to these cases. Also, numerical comparisons between standard Newton-Raphson strategies and the one presented here may be investigated. Finally, this methodology will be extended to more accurate models by considering a multi-group description for the radiation transport.

Appendix A: Stability of the State $T_i = T_e = T_r$.

Property 14 *All states such that $T_i = T_e = T_r$ are equilibrium states (in the 0D case (no spatial variation) case with no source term).*

Proof We only consider here the simplified the 0D case (no spatial variation) (no spatial dependence) with no source terms. Setting

$$X = \begin{pmatrix} E_r \\ E_e \\ E_i \end{pmatrix}, \qquad F(X) = \begin{pmatrix} c\sigma_P(\phi_e - \phi_r) \\ c\sigma_P(\phi_r - \phi_e) + \kappa(T_i - T_e) \\ \kappa(T_e - T_i) \end{pmatrix},$$

the model (1) writes under the following ordinary differential set of equations

$$\dot{X} = F(X).$$

The unique fix point X_0 such that $F(X_0) = 0$ corresponds to the case of equal temperatures $T_r = T_e = T_i$. Now, considering the case of a small perturbation δX around the equilibrium state X_0, one obtains

$$(X_0 \dot{+} \delta X) = \delta\dot{X} = F(X_0 + \delta X) \simeq F(X_0) + \partial_X F|_{X_0}\delta X = \partial_X F|_{X_0}\delta X.$$

In this linear case, the following analytical expression of δX is obtained

$$\delta X(t) = e^{\partial_X F|_{X_0} t}\delta X(0).$$

The study of the eigenvalues of the matrix s $\partial_X F|_{X_0}$ shows that the matrix displays two negative eigenvalues and a third one which is zero. Therefore, X_0 is a stable equilibrium. □

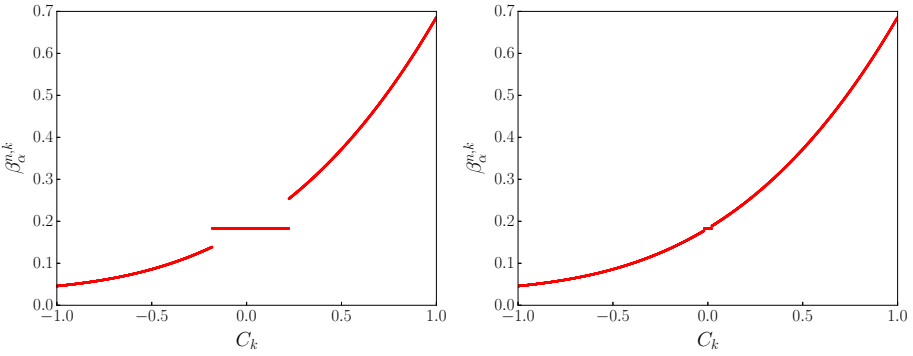

(a) $\epsilon = 0.1$. **(b)** $\epsilon = 0.01$.

Fig. 15 Representation of β_α^k a function of C_k using a constant reconstruction

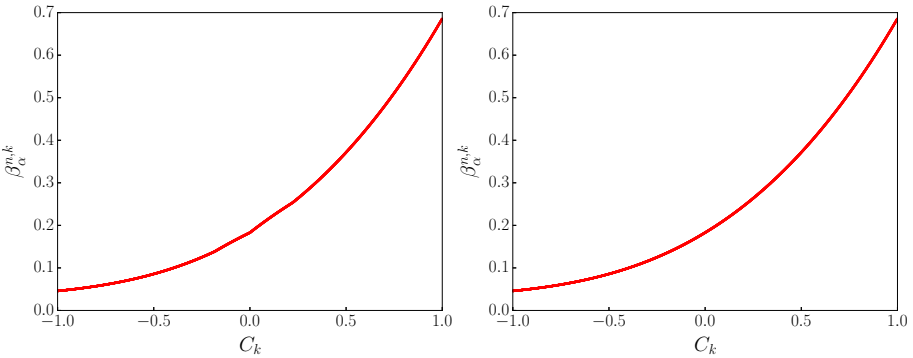

(a) $\epsilon = 0.1$. **(b)** $\epsilon = 0.01$.

Fig. 16 Representation of β_α^k a function of C_k using a linear reconstruction

Appendix B: Practical Computation of the Terms β_α^k and δ_{ie}^k

The evaluations of the expressions (14) may be sensitive if the denominators become close to zero. However this difficulty is only numerical. Indeed, performing a Taylor expansion on β_α^k in $T_\alpha^k = T_\alpha^n$ gives

$$\lim_{|T_\alpha^k - T_\alpha^n| \to 0} \beta_\alpha^k = \frac{4a(T_\alpha^n)^3}{\rho C_{v,\alpha}}. \tag{31}$$

Similarly, a Taylor expansion on δ_{ie}^k in $\phi_i^k = \phi_e^k$ leads to

$$\lim_{|T_i^k - T_e^k| \to 0} \delta_{ie}^k = \frac{1}{4a(T_e^k)^3}. \tag{32}$$

Coming back to the computation of β_α^k. The solution we consider consist in comparing the quantity $C_k = |T_\alpha^k - T_\alpha^n|/(T_\alpha^k + T_\alpha^n)$ with a threshold value ε. If C_k is found larger than ε then (14) is used otherwise one takes the expressions (31). In Fig. 15a, the value of β_α^k is displayed as function of the value of C_k for a large value of ε (left) and a small value of ε (right). Even for small ε one observes a discontinuity between the limit value and the definition of β_α^k. In

order to avoid this, one considers a linear reconstruction instead of a constant state. The limit value and the value in ε are simply connected using a linear approximation. In Fig. 16a, it is observed that the discontinuity vanishes even using large value of ε.

The same procedure is applied for coefficient δ_{ie}^{k}.

Remark In practice, it has been observed that using this linear reconstruction procedure, the choice of the value of ε does not have any impacts on the numerical results.

Appendix C: Temporal Discretisation of σ_P, κ and σ_R

In the case of an explicit discretisation, they are fixed at time t^n during the iterative process. In the implicit case, the quantity are computed at iteration $k+1$ while these coefficients are taken at step k. A third discretisation is studied, taking the half sum between the quantity at iteration k and time t^n. It is observed that taking small time steps all the discretisation give the same correct results. However, when using very large time step some differences appear. For example in Fig. 17, reconsidering the test case Marshak2A with large time step (only 100 time step and a coarse grid of 100 cells), it is observed that the explicit method is by far the less accurate while the implicit give the best accuracy. However, when looking at the computational time in Table 3, it is observed that the explicit method is the fastest while the implicit is the slowest.

Remark The results displayed in Fig. 17 are obtained using the conjugate gradient method. We mention that the results are very similar when using the Jacobi and Gauss–Seidel numerical schemes.

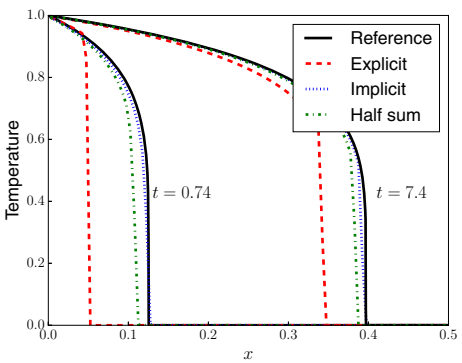

Fig. 17 Temperature comparisons between different time discretisations of σ_P, κ and σ_R for the test case Marshak2A using the gradient conjugate method

Table 3 Computational time (in second) for different time discretisations

	Explicit	Implicit	Half sum
Jacobi	22.4	24.9	36.7
Conjugate gradient	2.7	5.2	6.1
Hybrid-Jacobi	2.6	4.7	5.4

References

1. Decoster, A.: Fluids equations and transport coefficients of plasmas. Modeling of collisions, Series in applied Mathematics. ISBN: 2-84299-055-2 (1998)
2. Enaux, C.: Personnal communication (2018)
3. Evans, T.M., Densmore, J.D.: Methods for coupling radiation, ion and electron energies in grey implicit Monte Carlo. J. Comput. Phys. **225**, 1695–1720 (2007)
4. Fatenejad, M., Fryxell, B., Wohlbier, J., Myra, E., Lamb, D., Fryer, C., Graziani, C.: Collaborative comparison of simulation codes for high-energy-density physics applications. High Energy Density Phys. **9**, 63–66 (2013)
5. Feng, T., An, H., Yu, X., Li, Q., Zhang, R.: On linearization and preconditioning for radiation diffusion coupled to material thermal conduction equations. J. Comput. Phys. **236**, 28–40 (2013)
6. Fleck, J.A., Cummings, J.D.: An implicit Monte Carlo scheme for calculating time and frequency dependent nonlinear radiation transport. J. Comput. Phys. **8**(3), 313–342 (1971)
7. Fraley, G.S., Linnebur, E.J., Mason, R.J., Morse, R.L.: Thermonuclear burn characteristic of compressed deuterium-tritium microspheres. Phys. Fluids **17**(2), 474–489 (1974)
8. Knoll, D.A., Lowrie, R.B., Morel, J.E.: Numerical analysis of time integration errors for nonequilibrium radiation diffusion. J. Comput. Phys. **226**, 1332–1347 (2007)
9. Larsen, E.W., Mercier, B.: Analysis of a Monte Carlo method for nonlinear radiative transfer. J. Comput. Phys. **71**, 50–64 (1987)
10. Matteo, T.D., Blackman, E., Fabian, A.: Two temperature coronae in active galactic nuclei. Mon. Not. R. Astron. Soc. **291**, L23–L27 (1997)
11. Mihalas, D., Mihalas, B.: Foundations of Radiation Hydrodynamics. Oxford University Press, Oxford (1984)
12. Mousseau, V.A., Knoll, D.A.: New physical-based preconditioning of implicit methods for non-equilibrium radiation diffusion. J. Comput. Phys. **190**, 42–51 (2003)
13. Sijoy, C.D., Chaturvedi, S.: TRHD: three-temeprature radiation-hydrodynamics code with an implicit non-equilibrium radiation transport using a cell-centered monotonic finite volume scheme on unstructured-grids. Comput. Phys. Commun. **190**, 98–119 (2015)
14. Spitzer, L., Härm, R.: Transport phenomena in a completely ionized gas. Phys. Rev. **89**, 977–981 (1953)
15. Urbatsch, T.J., Evans, T.M.: Milagro Version 2. An implicit Monte Carlo code for thermal radiative transfer: capabilities, development, and usage. LA-14195-MS (2006)
16. Wollaber, A.B., Larsen, E.W., Densmore, J.D.: A discrete maximum principle for the implicit Monte Carlo equations. Nucl. Sci. Eng. **173**, 259–275 (2013)